CORPUS PUBLISHERS

Journal of Mineral and Material Science (JMMS)

ISSN: 2833-3616

Volume 3 Issue 3, 2022

Article Information

Received date: Aug 08, 2022

Published date: Aug 22, 2021

*Corresponding author

Nguyen Quang Hoc, Hanoi National University of Education, 136 Xuan Thuy, Cau Giay, Hanoi, Vietnam,

Email: hocnq@hnue.edu.vn

Keyword

Interstitial Alloy; Nonlinear and Elastic Defomation; Statistical Moment Method; W and WSi

Research Article

Young Modulus, Maximum Real Stress and Elastic Deformation Limit of W and WSi from Statistical Moment Method

Nguyen Quang Hoc[1*], Nguyen Duc Hien[2] and Nguyen Thi Hoa[3]

[1]*Hanoi National University of Education, 136 Xuan Thuy, Cau Giay, Hanoi, Vietnam*

[2]*Mac Dinh Chi High School, Chu Pah, Gia Lai, Vietnam*

[3]*University of Transport and Communications, 3 Cau Giay, Dong Da, Hanoi, Vietnam*

Abstract

We present the theory of nonlinear and elastic defomation for BCC metal and binary interstitial alloy builded on the basis of a statistical moment method and our numerical calculations for W and WSi depending on temperature, pressure and interstitial atom concentrations. Our numerical calculations for Young modulus of W are compared with experiments and our other numerical calculations are new and predictic.

Introduction

Metals and interstitial alloys are materials that have many applications and are of interest to many researchers. Recently, there are studies on the nonlinear and elastic deformation of these materials by the Statistical Moment Method (SMM) [1-22]. SMM calculations [23] on the pressure and the interstitial atomic concentration dependences of melting temperature for tungsten (W) and tungsten silicide (WSi) are in rather good agreement with experiments [24,25], Molecular Dynamics (MD) calculations [26,27], dislocation calculations [28] and Calculations of Phase Diagram (CALPHAD) [29]. The melting temperature, the jumps of volume, enthalpy and entropy at the melting point and the Debye temperature for WSi under pressure are studied by SMM [30]. The melting temperature of defective transition metals up to 400 GPa also determined by SMM [31]. In studying nonlinear and elastic deformation of materials like metals and alloys,there still are many other theoretical methods such as Molecular Dynamics (MD) method for example in studying the temperature dependence of Young modulus for metals [32], Finite Element Method (FET) for example in simulating flow during deep drawing of carbon alloy steel [33], first principles calculation method (or ab initio method) for example in studying elastic moduli of Fe [34], Tight-Binding (TB) Hamiltonian method for example in studying elastic moduli and constants of HCP and BCC crystals [35], Functional Density Theory (DFT) for example in studying alloy FeC [36], Calculation of Phase Diagram (CALPHAD) method for example in studying calometric assessment of alloys CuSi and AlCuSi [37], Modified Embedded Atom Method (MEAM) for example in studying [38], etc. In this paper, we present formulas in our nonlinear and elastic deformation theory for numerical calculations and numerical results for the Young modulus, the maximum real stress and the elastic strain limit of W and WSi.

Calculation Method and Numerical Results

In our model for BCC interstitial alloy AB with condition $c_B << c_A$ ($c_X = \frac{N_X}{N}$ (X = A, B) is the concentration of atoms X, N_X is the number of atoms X, $N=N_A+N_B$ is the total number of atoms of the alloy AB), the interstitial atom B stays at face center, the main metal atom A called as A_1 stays at body center and the main metal atom A called as A_2 stays at vertice of cubic unit cell [2,6-8,10,11,13,14,18,22]. In order to study nonlinear and elastic properties of BCC alloy AB by SMM, first we have to calculate the mean nearest neighbour distance between two atoms A in the alloy before deformation according to the following formula [2,39,40].

$$\overline{r_{1A}(P,T)} = \overline{r_{01A}(P,0)} + \overline{y(P,T)}, \overline{r_{01A}(P,0)} = (1-c_B)r_{01A}(P,0) + c_B r'_{01A}(P,0),$$

$$\overline{y(P,T)} = \sum_X c_X y_X(P,T),\ r'_{01A}(P,0) = \sqrt{3} r_{01B}(P,0),$$

$$r_{1B}(P,T) = r_{01B}(P,0) + y_{A_1}(P,T), r_{1A}(P,T) = r_{01A}(P,0) + y_A(P,T),$$

$$r_{1A_1}(P,T) = r_{1B}(P,T),\ r_{1A_2}(P,T) = r_{01A_2}(P,0) + y_B(P,T).$$

$$y_X(P,T) = \sqrt{\frac{2\gamma_X(P,0)\theta^2}{3k_X^3(P,0)} A_X(P,T)},\ A_X(P,T) = a_{1X}(P,T) + \sum_{i=2}^{6}\left(\frac{\gamma_X(P,0)\theta}{k_X^2(P,0)}\right)^i a_{iX}(P,T), \quad (1)$$

$$Y_X \equiv x_X \coth x_X, x_X = \frac{\hbar}{2\theta}\sqrt{\frac{k_X}{m_X}}.$$

$$a_{1X} = 1 + \frac{1}{2}Y_X, a_{2X} = \frac{13}{3} + \frac{47}{6}Y_X + \frac{23}{6}Y_X^2 + \frac{1}{2}Y_X^3,$$

$$a_{3X} = -\left(\frac{25}{3} + \frac{121}{6}Y_X + \frac{50}{3}Y_X^2 + \frac{16}{3}Y_X^3 + \frac{1}{2}Y_X^4\right),$$

How to cite this article: Hoc NQ, Hien ND and Hoa NT (2022) Young Modulus, Maximum Real Stress and Elastic Deformation Limit of W and WSi from Statistical Moment Method. J Miner Sci Materials 3: 1044

$$a_{4X} = \frac{43}{3} + \frac{93}{2}Y_X + \frac{169}{3}Y_X^2 + \frac{83}{3}Y_X^3 + \frac{22}{3}Y_X^4 + \frac{1}{2}Y_X^5,$$

$$a_{5X} = -\left(\frac{103}{3} + \frac{749}{6}Y_X + \frac{363}{2}Y_X^2 + \frac{391}{3}Y_X^3 + \frac{148}{3}Y_X^4 + \frac{53}{6}Y_X^5 + \frac{1}{2}Y_X^6\right),$$

$$a_{6X} = 65 + \frac{561}{2}Y_X + \frac{1489}{3}Y_X^2 + \frac{927}{2}Y_X^3 + \frac{733}{3}Y_X^4 + \frac{145}{2}Y_X^5 + \frac{31}{3}Y_X^6 + \frac{1}{2}Y_X^7.$$

Here, $\overline{r_{1A}(P,T)} \equiv a_{1A}(P,T)$ is the mean nearest neighbor distance between two atoms A in the alloy at pressure P and temperature T, $\overline{r_{01A}(P,0)} \equiv a_{01A}(P,0)$ is the mean nearest neighbor distance between two atoms A in the alloy at pressure P and temperature T = 0K, $\overline{y(P,T)}$ is the mean displacement of atom A in the alloy at pressure P and temperature T from equilibrium position, r_{01} $(P,\ )$ is the nearest neighbor distance between two atoms A in the pure metal A at pressure P and temperature T = 0K, $r'_{01A}(P,0)$ is the nearest neighbor distance between two atoms A in the zone containing the interstitial atom B at pressure P and temperature T = 0K, $y_X(P,T)$ is displacement of atom X(X = A, A_1, A_2, B) in the alloy at pressure P and temperature T from equilibrium position, $r_{1X}(P,T)$ is the nearest neighbour distance between two atoms A in the pure metal A or between atom X and other atom in the alloy at pressure P and temperature T, $r_{01X}(P,0)$ is the nearest neighbor distance between two atoms A in the pure metal A or between atom X and other atom in the alloy at pressure P and temperature

$$Pv_{0X} = -r_{01X}\left(\frac{1}{6}\frac{\partial \grave{u}_{0X}}{\partial r_{01X}} + \frac{\hbar\ \ {}_{0X}}{4k_X}\frac{\partial k_X}{\partial r_{01X}}\right), \tag{2}$$

Where $r_{01X} \equiv r_{01X}(P,0)$, $v_{0X} = \dfrac{4r_{01X}^3}{3\sqrt{3}}$ is the volume of cubic unit cell per atom X at pressure P and temperature T = 0K, $\grave{u}_{0X} = \sqrt{k_X(P,0)/m_X}$ is the vibrational frequency of the atom X at pressure P and temperature T = 0K,

$c_X = \dfrac{N_X}{N}, N = N_A + N_{A_1} + N_{A_2} + N_B$ is the total number of atoms in the alloy, $\theta = k_{\mathrm{Bo}}T, k_{\mathrm{Bo}}$ is the Boltzmann constant, $\hbar = h/(2\pi), h$ is the Planck constant, $\omega_X(P,T) = \sqrt{k_X(P,T)/m_X}$ is the vibrational frequency of the atom X at pressure P and temperature T, m_X is the mass of the atom X, u_{0X}, k_X, γ_{1X}, γ_{2X} and γ_X are the cohesive energy and the crystal parameters (k_X is the harmonic crystal parameter, γ_{1X}, γ_{2X} and γ_X are the anharmonic crystal parameters) of an atom X in the metal A or alloy AB [39,40]

$$u_{0X} = \frac{1}{2}\sum_{i=1}^{n_i}\varphi_{i0},\quad k_X = \frac{1}{2}\sum_{i=1}^{n_i}\left(\frac{\partial^2\varphi_{i0}}{\partial u_{i\beta}^2}\right)_{eq} = m_X\omega_X^2,$$

$$\gamma_X = 4(\gamma_{1X} + \gamma_{2X}), \gamma_{1X} = \frac{1}{48}\sum_{i=1}^{n_i}\left(\frac{\partial^4\varphi_{i0}}{\partial u_{i\beta}^4}\right)_{eq}, \gamma_{2X} = \frac{6}{48}\sum_{\substack{i=1\\ \alpha\neq\beta}}^{n_i}\left(\frac{\partial^4\varphi_{i0}}{\partial u_{i\alpha}^2\partial u_{i\beta}^2}\right)_{eq}, \tag{3}$$

Where $u_{i\beta}(\beta = x, y, z)$ is the displacement of the ith particle from the equilibrium position in the direction β, φ_{i0} is the interaction potential between 0th particle and the ith particle and (…)eq is the value of (…) at the equilibrium position.

The values of u_{0X}, k_X, γ_{1X}, γ_{2X} and γ_X are calculated in terms of the number of atoms and the coordinates of atoms on coordination spheres [18,39,40]. In Eq. (3). n_i is the number of atoms on the ith coordination sphere. The radii of the first coordination sphere is the nearest neighbor distance between two atoms. Then, the nearest neighbor distance and the mean nearest neighbor distance between two atoms within the framework of SMM take into account the anharmonicity of lattice vibrations. Assume ε is the strain of the alloy AB. The mean nearest neighbor distances between two atoms A in the alloy after deformation at pressure P and temperature T = 0K and at pressure P and temperature T respectively are determined by [7,18,42,43]

$$a_{01X}^{F}(P,0) = a_{01X}(P,0)(1+\varepsilon),$$
$$a_{1X}^{F}(P,T) = a_{1X}(P,T) + \varepsilon . a_{01X}(P,0)(2+\varepsilon). \tag{4}$$

The Helmholtz free energies of the alloy AB before and after deformation have the form [7,18,39-43]

$$\Psi_{AB} = N\psi_{AB} = N\left(\sum_X c_X \psi_X - TS_c^{AB}\right),$$
$$\Psi_X = N\psi_X = U_{0X} + \Psi_{0X} + 3N\left\{\frac{\theta^2}{k_X^2}\left[\gamma_{2X}Y_X^2 - \frac{2\gamma_{1X}}{3}\left(1+\frac{Y_X}{2}\right)\right] + \right.$$
$$\left. + \frac{2\theta^3}{k_X^4}\left[\frac{4}{3}\gamma_{2X}^2 Y_X\left(1+\frac{Y_X}{2}\right) - 2\left(\gamma_{1X}^2 + 2\gamma_{1X}\gamma_{2X}\right)\left(1+\frac{Y_X}{2}\right)(1+Y_X)\right]\right\},$$
$$\Psi_{0X} = 3N\theta\left[x_X + \ln\left(1-e^{-2x_X}\right)\right],$$
$$\Psi_{AB}^{F} = N\left(\sum_X c_X \psi_X^F - TS_c^{ABF}\right), \tag{5}$$
$$\Psi_X^F \approx U_{0X}^F + \Psi_{0X}^F + 3N\left\{\frac{\theta^2}{k_X^{F2}}\left[\gamma_{2X}^F Y_X^{F2} - \frac{2\gamma_{1X}^F}{3}\left(1+\frac{Y_X^F}{2}\right)\right] + \right.$$
$$\left. + \frac{2\theta^3}{k_X^{F4}}\left[\frac{4}{3}\gamma_{2X}^{F2} Y_X^F\left(1+\frac{Y_X^F}{2}\right) - 2\left(\gamma_{1X}^{F2} + 2\gamma_{1X}^F\gamma_{2X}^F\right)\left(1+\frac{Y_X^F}{2}\right)\left(1+Y_X^F\right)\right]\right\},$$
$$\Psi_{0X}^F = 3N\theta\left[x_X^F + \ln(1-e^{-2x_X^F})\right],$$

Where $c_A = 1 - 7c_B$, $c_{A_1} = 2c_B$, $c_{A_2} = 4c_B$, ψ_X and ψ_X^F are the Helmholtz free energies of the atom X alloy AB before and after deformation, S_c^{AB} and S_c^{ABF} are the configurational entropies of the alloy AB before and after deformation and are considered equal. The Young modulus of the alloy AB is given by [18,40]

$$E_{YAB} = E_{YA} \frac{\sum_X c_X \frac{\partial^2 \psi_X}{\partial \varepsilon^2}}{\frac{\partial^2 \psi_A}{\partial \varepsilon^2}}, \quad E_A = \frac{1}{\pi . a_{1A} B_{1A}}, \quad B_{1A} = \frac{1}{k_A}\left[1 + \frac{2\gamma_A^2 \theta^2}{k_A^4}\left(1 + \frac{1}{2}Y_A\right)(1 + Y_A)\right],$$

$$\frac{1}{3}\frac{\partial^2 \psi_X}{\partial \varepsilon^2} = \left\{\frac{2}{3}\frac{\partial^2 u_{0X}}{\partial a_{1X}^2} + \frac{\hbar \omega_X}{k_X}\left[\frac{\partial^2 k_X}{\partial a_{1X}^2} - \frac{1}{2k_X}\left(\frac{\partial k_X}{\partial a_{1X}}\right)^2\right]\right\} a_{01X}^2 + \\ + \left(\frac{\partial u_{0X}}{\partial a_{1X}} + \frac{3\hbar \omega_X \coth x_X}{2k_X}\frac{\partial k_X}{\partial a_{1X}}\right) a_{01X}. \tag{6}$$

Here, E_{YA} is the Young modulus of the pure metal A. In the nonlinear deformation of the alloy AB, the relationship between the stress and the strain is described as exponential [7,18,42,43]

$$\sigma_{AB} = \sigma_{0AB} \frac{\varepsilon^{\alpha_{AB}}}{1 + \varepsilon}, \tag{7}$$

where σ_{0AB} and α_{AB} are constants.

The strain energy density of the alloy AB is defined by [7,18,42,43]

$$f_{AB}(\varepsilon) = \frac{\Psi_{AB}^F}{V_{AB}^F} - \frac{\Psi_{AB}}{V_{AB}} = \sum_X c_X \left(\frac{\psi_X^F}{v_{AB}^F} - \frac{\psi_X}{v_{AB}}\right) = \\ = \sum_X c_X \left\{\psi_X \left(\frac{1}{v_{AB}^F} - \frac{1}{v_{AB}}\right) + \frac{2\varepsilon a_{01X}^F}{v_{AB}^F}\left(\frac{\partial \psi_X^F}{\partial a_{1X}^F}\right)_T + \\ + \frac{\varepsilon^2}{2v_{Ab}^F}\left[\left(\frac{\partial^2 \psi_X^F}{\partial a_{1X}^{F2}}\right)_T \left(2a_{01X}^F\right)^2 + \left(\frac{\partial \psi_X^F}{\partial a_{1X}^F}\right)_T 2a_{01X}\right]\right\}., \tag{8}$$

$$\frac{1}{3}\left(\frac{\partial \psi_X^F}{\partial a_{1X}^F}\right)_T = \frac{1}{6}\frac{\partial u_{0X}^F}{\partial a_{1X}^F} + \frac{\theta Y_X^F}{2k_X^F}\frac{\partial k_X^F}{\partial a_{1X}^F},$$

$$\frac{1}{3}\left(\frac{\partial^2\psi_X^F}{\partial a_{1X}^{F2}}\right)_T = \frac{1}{6}\frac{\partial^2 u_{0X}^F}{\partial a_{1X}^{F2}} + \frac{\hbar\omega_X^F}{4k_X^F}\left[\frac{\partial^2 k_X^F}{\partial a_{1X}^{F2}} - \frac{1}{2k_X^F}\left(\frac{\partial k_X^F}{\partial a_{1X}^F}\right)^2\right].$$

When the strain velocity is constant,

$$f_{AB}(\varepsilon) = C_{AB}\sigma_{AB}\varepsilon, \tag{9}$$

where C_{AB} is a proportional factor [7,18,42,43]. Assume the maximum value $f_{AB\max}$ corresponds to the strain ε_F. Therefore,

$$f_{AB}(\varepsilon_F) = f_{AB\max} = C_{AB}\sigma_{AB\max}\varepsilon_F. \tag{10}$$

The maximum values of the stress $\sigma_{AB\max}$ and the real stress $\sigma_{1AB\max}$ are [7,18,42,43]

$$\sigma_{AB\max} = \frac{f_{AB\max}}{C_{AB}\varepsilon_F},$$

$$\sigma_{1AB\max} = \frac{\sigma_{AB\max}}{1+\varepsilon_F} = \frac{f_{AB\max}}{C_{AB}\varepsilon_F(1+\varepsilon_F)}. \tag{11}$$

The factor C_{AB} is determined from experimental data of stress $\sigma_{AB0.2}$ in the alloy AB in the form [7,18,42,43]

$$C_{AB} = \frac{f_{AB}(\varepsilon_{0,2})}{\sigma_{AB0,2}.\varepsilon_{0,2}}. \tag{12}$$

After having the value of the strain ε_F, we can calculate the constants σ_{0AB} and α_{AB}. From that we can determine the expression describing the stress-strain relationship in nonlinear deformation of alloy AB. The elastic strain limit of the alloy AB has the form [7,18,42,43]

$$\sigma_{ABe} = E_{YAB}\varepsilon_e = \sigma_{0AB}\frac{\varepsilon_e^{\alpha_{AB}}}{1+\varepsilon_e}. \tag{13}$$

When the interstitial atom concentration B is zero, the characteristic nonlinear elastic deformation quantities of the alloy AB become that of the pure metal A. We use the Mie-Lennard-Jones potential for W and WSi with potential parameters given in Table 1 [44-46]

$$\varphi(r) = \frac{D}{n-m}\left[m\left(\frac{r_0}{r}\right)^n - n\left(\frac{r_0}{r}\right)^m\right]. \tag{14}$$

Table 1: Potential parameters [45,46], experimental Poisson ratio and density [44,47] for W and Si.

Interaction	m	n	$D(10^{-16}\text{erg})$	$r_0(10^{-10}\text{m})$	ν	$\rho(g/cm^3)$
W-W [46]	4.06	8.58	25608.93	2.7365	0.28	19.257
Si-Si [45]	6	12	45128.34	2.295	0.28	2.329

Figures 1-4 describe the silicon concentration, pressure and temperature dependences of mean nearest neighbor distance a and volume V for W and WSi at $P = 0$ and at $T = 300$K calculated by SMM and other calculations [48]. The agreement between the SMM calculation and the other calculation [48] is very good especially in the low pressure region.

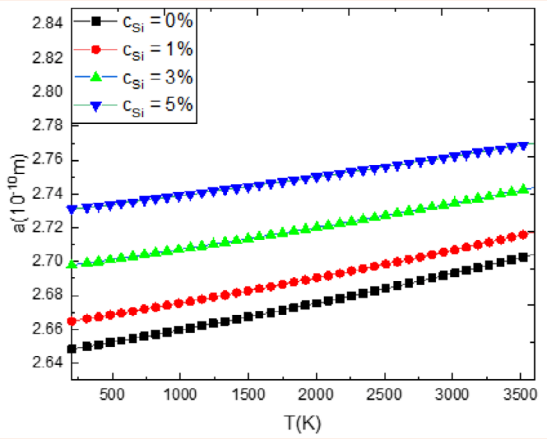

Figure 1: $a(T,c_{Si})$ for W and WSi at $P = 0$ calculated by SMM.

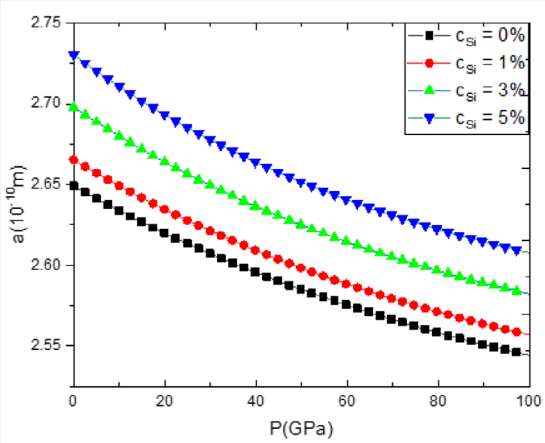

Figure 2: $a(P,c_{Si})$ for W and WSi at $T = 300$K calculated by SMM.

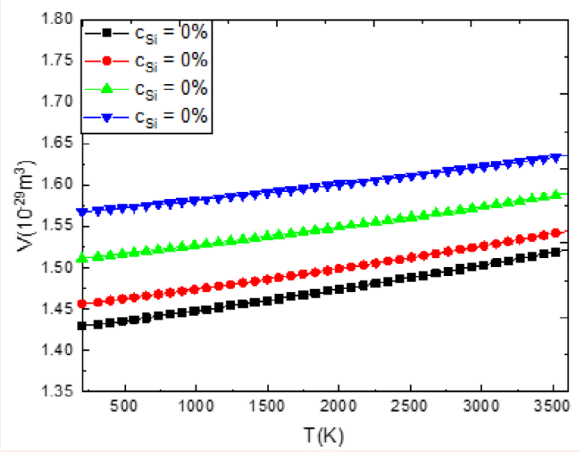

Figure 3: $V(T,c_{Si})$ for W and WSi at $P = 0$ calculated by SMM.

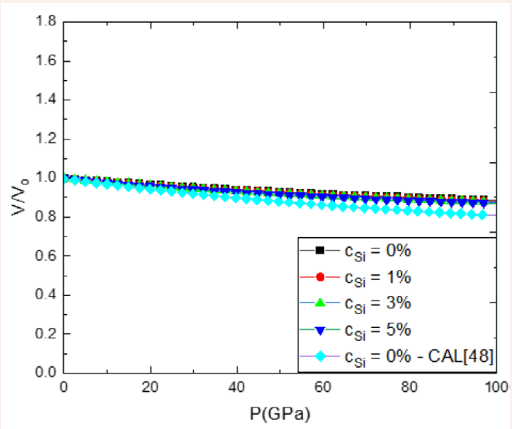

Figure 4: $V(P,c_{Si})$ for W and WSi at $T = 300$K calculated by SMM and from CAL[48].

Figures 5 & 6 show the silicon concentration, pressure and temperature dependences of Young modulus E_Y for W and WSi at $P = 0$ and at $T = 300$K calculated by SMM. The temperature dependences of E_Y for W at $P = 0$ calculated by SMM are in good agreement with experiments in the temperature range below 1000K [49]. The pressure dependences of E_Y for W at $T = 300$K calculated by SMM are in good agreement with experiments [52,54,55]. Values of E_Y for W at $T = 300$K, $P = 0$ calculated by SMM very well agree with experiments [50-52, 55-57] (Table 2).

Table 2: Young modulus E_Y of W at $T = 300$K, $P = 0$ calculated by SMM and from EXPT [47-49,50-52].

Method	*E*(GPa)
SMM	414.0
EXPT [50,52]	415.0
EXPT [55]	377.4
EXPT [56,57]	440.2
EXPT [51]	421.5

For W and WSi at the same P and c_{Si} when T increases, a increases and E_Y decreases. For W and WSi at the same T and c_{Si} when P increases, a decreases and E_Y increases. For W and WSi at the same T and P when c_{Si} increases, a increases and E_Y decreases.

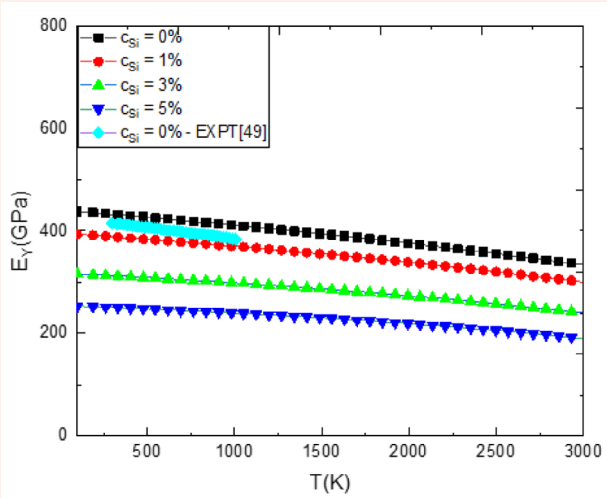

Figure 5: $E_Y(T,c_{Si})$ for W and WSi at $P = 0$ calculated by SMM and from EXPT [49].

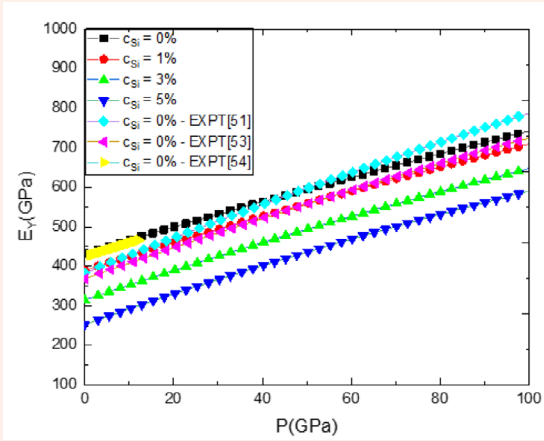

Figure 6: $E_Y(P,c_{Si})$ for W and WSi at $T = 300$K calculated by SMM and from EXPT [51,53,54].

At $P = 0$, we choose the experimentai stress values $\sigma_{0,2\%}$ for W and WSi at each temperature from experiments [58] according to the formula $\sigma_{0,2\%} = E.\varepsilon_{0,2\%}$. The graph of $f(\varepsilon)$ always exists $\varepsilon = \varepsilon_F$ such that f= f_{max} Namely when $c_{Si} = 0$, $\varepsilon_F = 8.3\%$ corresponding to f_{max} =16.79 GPa. When $c_{Si} = 1\%$, $\varepsilon_F = 8.1\%$ corresponding to $f_{max} = 35.57$ GPa. When $c_{Si} = 3\%$, $\varepsilon_F = 8.0\%$ corresponding to $f_{max} = 33.65$ GPa. From that, we calculate the values of the maximum real stress $\sigma_{1\max}$ and the elastic strain limit σ_e corresponding to the strain ε_e for W and WSi at T = 300K, P = 0 and different silicon concentrations as shown in Tables 3 & 4. Then, graphs of $f(\varepsilon, c_{Si})$ and $\sigma_1(\varepsilon, c_{Si})$ for W and WSi are depicted in Figure 7.

Table 3: Strain energy density $f(\varepsilon, c_{Si})$ and real stress $\sigma_1(\varepsilon, c_{Si})$ for W and WSi at $T = 300K$ and $P = 0$

$c_{Si} = 0$			$c_{Si} = 1\%$			$c_{Si} = 3\%$		
ε (%)	$f(\varepsilon)$ (GPa)	$\sigma_1(\varepsilon)$ (MPa)	ε (%)	$f(\varepsilon)$ (GPa)	$\sigma_1(\varepsilon)$ (MPa)	ε (%)	$f(\varepsilon)$ (GPa)	$\sigma_1(\varepsilon)$ (MPa)
0.01	0.02	439	0.01	0.02	431	0.01	0.02	394
0.14	0.32	537	0.16	0.35	530	0.2	0.41	491
0.5	1.43	589	0.5	1.36	575	0.5	1.23	524
1.0	3.58	618	1.0	3.41	603	1.0	3,08	548
1.5	6.24	635	1.5	5.95	619	1.5	5,39	562
2,0	9.27	646	2.0	8.84	629	2.0	8,02	572
2.5	12.52	654	2.5	11.94	636	2.5	10,84	578
3.0	15.87	660	3.0	15.14	642	3.0	13,75	583
3.5	19.23	664	3.5	18.35	646	3.5	16,68	587
4.0	22.52	668	4.0	21.49	650	4.0	19,53	590
4.5	25.67	671	4.5	24.49	652	4.5	22,26	592
5.0	28.61	673	5.0	27.3	654	5.0	24,81	594
5.5	31.31	675	5.5	29.87	656	5.5	27.14	596
6.0	33.71	676	6.0	32.16	657,21	6,0	29.2	597
6.5	35.79	677	6.5	34.13	658,06	6.5	30.96	597
7.0	37,50	678	7.0	35.74	658,63	7.0	32.36	598
7.5	38.8	678	7.5	36.91	658,97	7.8	33.62	598
8.0	39.57	678	8.0	37.53	659,10	8.0	33.65	598
8.1	39.65	678	8.1	37.57	659,10	8.1	33.6	598
8.2	39.69	678	8.2	37.56	659,10	8.2	33.49	598
8.3	39.7	678	8.3	37.5	659,09	8.3	33.31	598
8.4	39.66	678	8.4	37.38	659	8.4	33.03	598
8.45	39.62	678	8.45	37.29	659	8.45	32.85	598

Table 4: $\varepsilon_F(c_{Si})$ corresponding to $f_{max}(c_{Si})$, $\sigma_{1max}(c_{Si})$ and $\sigma_e(c_{Si})$ corresponding to $\varepsilon_e(c_{Si})$ for W and WSi at T = 300K and P= 0

c_{Si} (%)	σ_{1max} (MPa)	ε_F (%)	σ_e (MPa)	ε_e (%)
0	678	8.3	538	0.14
1	659	8.1	531	0.16
3	598	8.0	490	0.20

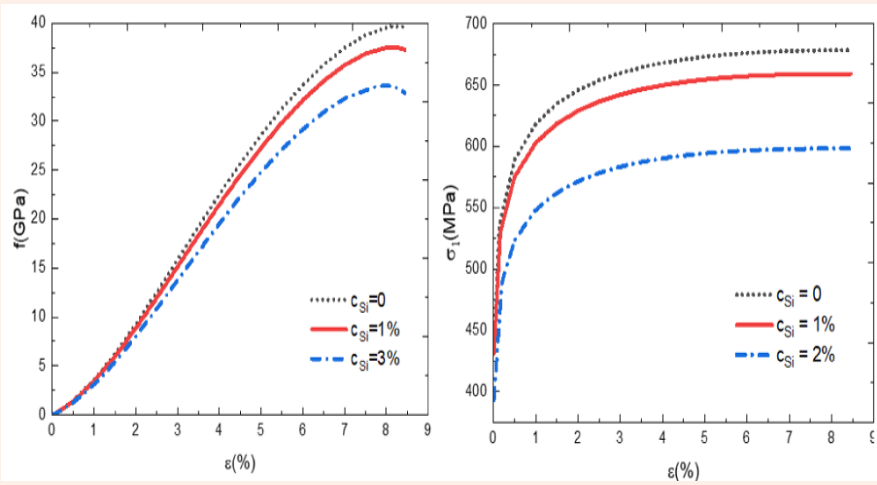

Figure 7: (a) $f(\varepsilon, c_{Si})$ and (b) $\sigma_1(\varepsilon, c_{Si})$ for W and WSi at T = 300K and P = 0

The values of $f(\varepsilon)$ and $\sigma_1(\varepsilon)$ for WSi at P = 0, c_{Si} = 3% and different temperatures are summarised in Table 5. When T = 1000K, ε_F = 5.8% corresponds to f_{max} = 24.36 GPa. When T = 1500K, ε_F = 4.9% corresponds to f_{max} = 19.85 GPa. When T = 2000K, ε_F = 4.1% corresponds to f_{max} = 16.37 GPa. From that, we calculate the values of ε_F, σ_{1max}, σ_e and ε_e for WSi at c_{Si} = 3%, P = 0 and different temperatures as shown in Table 6. Then, graphs of $f(\varepsilon, T)$ and $\sigma_1(\varepsilon, T)$ for WSi are depicted in Figure 8.

Table 5: Strain energy density $f(\varepsilon, T)$ and real stress $\sigma_1(\varepsilon, T)$ for W and WSi at c_{Si} = 3% and P= 0

T = 1000K			T = 1500K			T = 2000K		
ε (%)	$f(\varepsilon)$ (GPa)	$\sigma_1(\varepsilon)$ (MPa)	ε (%)	$f(\varepsilon)$ (GPa)	$\sigma_1(\varepsilon)$ (MPa)	ε (%)	$f(\varepsilon)$ (GPa)	$\sigma_1(\varepsilon)$ (MPa)
0.01	0.02	455	0.01	0.02	466	0.01	0.02	484
0.25	0.55	542	0.29	0.69	544	0.36	0.93	555
0.5	1.28	561	0.5	1.32	556	0.5	1.38	562

1.0	3.13	580	1.0	3.19	572	1.0	3.27	574
1.5	5.39	590	1.5	5.43	580	1.5	5.51	581
2.0	7.92	597	2.0	7.91	585	2.0	7.94	584
2.5	10.59	601	2.5	10.48	588	2.5	10.42	587
3.0	13.3	604	3.0	13.03	590	3.0	12.83	588
3.5	15.94	606	3.5	15.46	592	3.5	14.97	589
4.0	18.43	608	3.7	16.37	592	3.6	15.34	589
4.5	20.69	609	4.0	1762	593	37	15,67	589,05
5.0	22.6	609	4.2	18,38	592,91	3,8	15.96	589
5.5	23.98	610	4.4	19.03	593	3.9	16.19	589
5.7	24.29	610	4.6	19.54	593	4.0	16.33	589
5.8	24.36	610	4.8	19.83	593	4.1	16.37	589
6.0	24.25	610	4.9	19.85	593	4.2	16.23	589
6.1	24.00	610	5.0	19.73	593	4.3	15.82	589
6.2	23.53	610	5.1	19.4	593	4.4	14.97	589
6.3	22.72	610	5.2	18.75	593	4.5	13.26	589
6.4	21.28	610	5.3	17.53	593	4.6	9.69	589
6.5	18.54	610	5.4	15.19	593	4.7	0.85	589

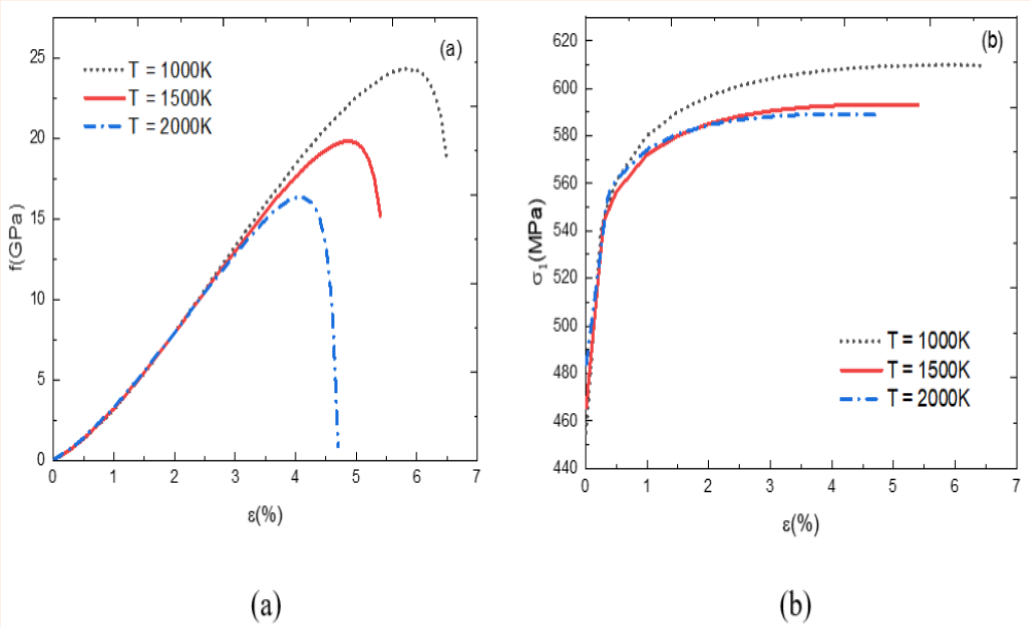

Figure 8: (a) $f(\varepsilon,T)$ and (b) $\sigma_1(\varepsilon,T)$ for WSi at c_{Si} = 3% and P = 0

Table 6: $\varepsilon_F(c_{Si})$ corresponding to $f_{max}(T)$, $\sigma_{1max}(T)$ and $\sigma_e(T)$ corresponding to $\varepsilon_e(T)$ for WSi at c_{Si} = 3%, *P*= 0 and different temperatures.

T(K)	σ_{1max} (MPa)	ε_F (%)	σ_e (MPa)	ε_e (%)
1000	610	5.8	542	0.25
1500	593	4.9	544	0.29
2000	589	4.1	555	0.36

The values of $f(\varepsilon)$ and $\sigma_1(\varepsilon)$ for WSi at *P*= 20GPa, *T* = 300K and different silicon concentrations are summarised in Table 7. When c_{Si} = 0, ε_F = 8.9% corresponds to f_{max} = 44.73 GPa. When c_{Si} = 1%, ε_F = 8.5% corresponds to f_{max} = 41.48 GPa. When ε_F = 3%, ε_F = 8.1% corresponds to f_{max} = 31.12 GPa. From that, we calculate the values of ε_F, σ_{1max}, σ_e and ε_e for W and WSi at P= 20GPa, T = 300K and different temperatures as shown in Table 8. Then, graphs of $f(\varepsilon, c_{Si})$ and $\sigma_1(\varepsilon, c_{Si})$ for W and WSi are depicted in Figure 9.

Table 7: Strain energy density $f(\varepsilon, c_{Si})$ and real stress $\sigma_1(\varepsilon, c_{Si})$ for W and WSi at *T* = 300K and *P* = 20 GPa.

c_{Si} = 0			c_{Si} =1%			c_{Si} =3%		
ε (%)	$f(\varepsilon)$ (GPa)	$\sigma_1(\varepsilon)$ (MPa)	ε (%)	$f(\varepsilon)$ (GPa)	$\sigma_1(\varepsilon)$ (MPa)	ε (%)	$f(\varepsilon)$ (GPa)	$\sigma_1(\varepsilon)$ (MPa)
0.01	0.01	443	0,01	0.01	442	0.01	0.003	415
0.12	0.15	542	0,13	0.13	540	0.15	0.1	507
0.5	1.01	607	0,5	0.89	597	0.5	0.67	553
1.0	2.93	639	1,0	2.68	628	1.0	2.2	580
1.5	5.54	658	1,5	5.14	645	1.5	4.38	595
2.0	8.64	670	2,0	8.09	656	2.0	7.02	605
2.5	12.07	679	2,5	11.35	664	2.5	9.99	612
3.0	15.68	686	3,0	14.81	671	3.0	13.13	617
4.0	23.02	695	4,0	21.82	679	4.0	19.54	625
5.0	29.9	701	5,0	28.41	685	5.0	25.54	629
5.5	33.02	704	5,5	31.37	687	5.5	28.23	631
6.0	35.85	705	6,0	34.05	6885	6.0	30.62	632
6.5	38.35	706	6.5	36.41	689	6.5	32.68	633
7.0	40.5	707	7	38.39	690	7.0	34.35	633
7.5	42.27	708	7,5	39.95	690	7.5	35.53	633

8.0	43.6	709	8	41.03	691	7.7	35.84	634
8.5	44.46	709	8.4	41.45	691	8.0	36.1	634
8.6	44.56	709	8.5	41.48	691	8.1	36.12	634
8.7	44.65	709	8.6	41.47	691	8.2	36.1	634
8.8	44.7	709	8.7	41.42	691	8.3	36.04	634
8.9	44.73	709	8.9	41.18	691	8.5	35.77	634
9.1	44.69	709	9.1	40.67	691	8.7	35.25	634
9.5	44.06	709	9.5	38.11	691	9.0	33.75	633
9.7	43.25	709	9.7	34.76	691	9.5	26.67	633
10	3971	708	10	11.31	690	9.7	18.41	633

Table 8: $\varepsilon_F(c_{Si})$ corresponding to $f_{max}(c_{Si})$, $\sigma_{1max}(c_{Si})$ and $\sigma_e(c_{Si})$ corresponding to $\varepsilon_e(c_{Si})$ for W and WSi at T = 300K and P = 20 GPa.

c_{Si} (%)	σ_{1max} (MPa)	σ_e (%)	σ_e (MPa)	ε_e (%)
0	709	8.9	542	0.12
1	691	8.5	540	0.13
3	634	8.1	507	0.15

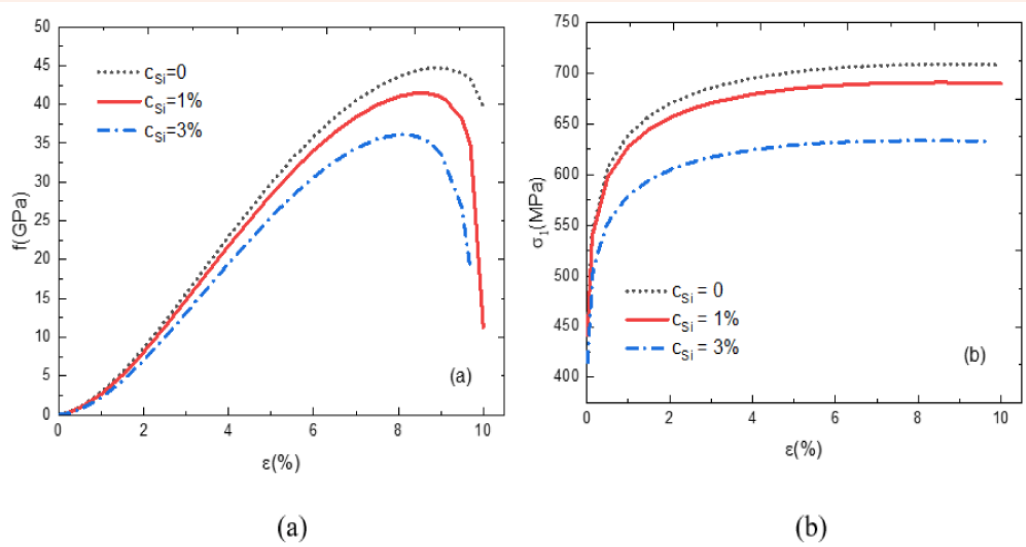

Figure 9: a) $f(\varepsilon, c_{Si})$ and (b) $\sigma_1(\varepsilon, c_{Si})$ for W and WSi at T = 300K and P = 20GPa.

According to the above SMM calculationds for WSi at the same pressure P and temperature T when the silicon concentration c_{Si} increases, the maximum real stress σ_{1max} and the elastic strain limit σ_e decrease. Namele for WSi at P = 0, T = 300K when c_{Si} increases from 0 to 3%, the strain energy density decreases and therefore, σ_{1max} decreases from 678.43 to 598.26 MPa and σ_e decreases from 537.86 to 490.39 MPa. For W and WSi at the same P and c_{Si} when T increases, σ_{1max} decreases and σ_e increases.

For example for WSi at $P = 0$, $c_{Si} = 3\%$ when T increases from 1000 to 2000K, σ_{1max} decreases from 609.8 to 589.16 MPa and σ_e increases from 541.6 to 555.49 MPa. This is in in good agreement with calculation law for metals [42] and substitutional alloys [43]. For W and WSi at the same T and c_{Si} when P increases, σ_{1max} and σ_e increase. For example for WSi at $T = 300K$, $c_{Si} = 3\%$ when P increases from 0 to 20 GPa, σ_{1max} increases from 598.26 to 633.66 MPa and σ_e increases from 490.39 to 507.21 MPa. This also is in in good agreement with calculation law for metals [42] and substitutional alloys [43].

Conclusion

The paper presents theoretical results and numerical calculations for nonlinear and elastic deformation quantities of W and WSi in the range from 200 to 3600K, from 0 to 100 GPa and from 0 to 5% of silicon concentration .using the Mie-Lennard-Jones potential and the coordination sphere method. The calculated results for the Young modulus of W are in good agreement with the experimental data and other calculations. The calculated results for WSi are predictive, orienting experimental results in the future.

Acknowledgment

This research is partly funded by University of Transport and Communications (UTC) under project number T2022-CB-010.

References

1. Hoc NQ, Tinh BD, Tuan LD, Hien ND (2016) Elastic deformation of binary and ternary interstitial alloys with FCC structure and zero pressure: Dependence on temperature, concentration of substitution atoms and concentration of interstitial atoms. Journal of Science of HNUE Mathematical and Physical Sciences 61(7): 47-57.
2. Hoc NQ, Hien ND (2017) Study on elastic deformation of interstitial alloy AB with BCC structure under pressure. Proc of the 10th National Conference on Solid State Physics and Material Science (SPMS), Hue City, Vietnam, 19-21, pp. 911-914.
3. Hoc NQ, Hoa NT, Hien ND (2017) Study on elastic deformation of substitution alloy AB with interstitrial atom C and BCC structure under pressure. Scientific Journal of Hanoi Metropolitan University, Natural Science and Technology 20: 55-66.
4. Học NQ, Hien ND (2018) Study on elastic deformation of substitution alloy AB with interstitrial atom C and FCC structure under pressure. Hnue Journal of Science, Natural Sciences 63(3): 23-33.
5. Hoc QN, Hien DN (2018) Study on elastic deformation of substitution alloy AB with interstitrial atom C and BCC structure under pressure. 42nd Vietnam National Conference on Theoretical Physics (NCTP-42), IOP Conf. Series: Journal of Physics: Conf Series 1034: 012005.
6. Tinh BD, Hoc NQ, Vinh DQ, Cuong TD, Hien ND (2018) Thermodynamic and elastic properties of interstitial alloy FeC with BCC structure at zero pressure. Advances in Materials Science and Engineering.
7. Hoc NQ, Hoa NT, Hien ND, Thang DQ (2018) Study on nonlinear deformation of binary interstitial alloy with BCC structure under pressure. HNUE Journal of Science, Natural Sciences 63(6): 57-65.
8. Hoc NQ, Hien ND, Thang DQ (2018) Elastic deformation of alloy FeSi with BCC structure under pressure. HNUE Journal of Science, Natural Sciences 63(6): 74-83.
9. Hoc NQ, Tinh BD, Nguyen Duc, Hien ND (2019) Elastic moduli and elastic constants of interstitial alloy AuCuSi with FCC structure under pressure. High Temperature Materials and Processes 38: 264-272.
10. Hoc NQ, Cuong TD, Hien ND (2019) Study on elastic deformation of interstitial alloy FeC with BCC structure under pressure. Proc the ACCMS-Theme Meeting on "Multiscale Modelling of Materials for Sustainable Development", VNU, Hanoi, Vietnam, VNU Journal of Sciences: Mathematics-Physics 35(1): 1-12.
11. Hoc NQ, Hoa NT, Cuong TD, Thang DQ (2019) On the melting of interstitial alloys FeH, FeSi and FeC with a bcc structure under pressure. Proc the ACCMS-Theme Meeting on "Multiscale Modelling of Materials for Sustainable Development", VNU, Hanoi, Vietnam, Vietnam Journal of Science, Technology and Engineering 61(2): 17-22.
12. Hoc NQ, Hoa NT, Hien ND (2019) Build the theory of nonlinear deformation for BCC and FCC substitutional alloys AB with interstitial atom C under pressure. HNUE Journal of Science, Natural Sciences 64(6): 45-56.

13. Hoc NQ, Tinh BD, Hien ND (2020) Stress-strain curve of FCC interstitial alloy AuSi under pressure. Romanian Journal of Physics 65(5-6): 608.

14. Hoc NQ, Hien ND, Hoa NM, Trung VQ (2020) Combining the Mie-Lennard-Jones and the model atomic potentials in studying the elastic deformation of interstitial alloy FeSi with BCC structure under pressure. HNUE Journal of Science, Natural Sciences 65(6): 61-74.

15. Hoc NQ, Hien ND, Hoa NM, Vu Quoc Trung (2021) Combining the Mie-Lennard-Jones and the Morse potentials in studying the elastic deformation of interstitial alloy AgC with FCC structure under pressure. VNU Journal of Sciences: Mathematics-Physics 37(2): 31-42.

16. Hoc NQ, Tinh BD, Hien ND, Gelu Coman G (2021) Study on nonlinear deformation of FCC-AuCuSi under pressure by the statistical moment method. Advanced Materials Science and Engineering 2021: 6693326.

17. Hoc NQ, Hien ND, Nam TD, Thanh VL (2021) Study on elastic deformation of stainless steel under pressure. HNUE Journal of Science, Natural Sciences 66(2): 83-99.

18. Hoc NQ, Tinh BD, Hien ND, Coman G (2021) Nonlinear deformation of BCC metal Fe and BCC interstitial alloy FeSi: Dependence on temperature, pressure and silicon concentration. Materials Physics and Mechanics 47: 501-513.

19. Hoc NQ, Hien ND, Hoa NT, Uyen PP, Ngoc TH (2022) Elastic deformation and elastic wave velocity of ternary alloys FeCrSi and AuCuSi. HNUE Journal of Science, Natural Sciences 67(1): 38-53.

20. Hoa NT, Hoc NQ, Hien ND (2022) Study on elastic deformation of FCC binary substitutional alloys at zero pressure. Science Journal of Transport 12: 35-41.

21. Hoc NQ, Hien ND (2022) Nonlinear deformation of Au, AuSi and AuCuSi with FCC structure under pressure. HNUE Journal of Science, Natural Sciences 67(2): 40-54.

22. Hoc NQ, Hien ND, Vi TK (2022) Elastic deformation and velocity of elastic wave for metal Fe and its interstitial alloys with BCC structure: Dependence on temperature, pressure and concentration of interstitial atoms. Physica B.

23. Hoc NQ, Cuong TD, Tinh BD, Viet LH (2019) Study on the melting of the defective interstitial alloys TaSi and WSi with BCC structure. Journal of the Korean Physical Society 74: 801-805.

24. Vereshchagin LF, Fateeva NS (1977) Melting temperatures of refractory metals at high pressures. High Temperature High Pressure 9: 619-628.

25. Errandonea D, Schwager B, Ditz R, Gessmann C, Boehler R, et al. (2001), Systematics of transition-metal melting. Physical Review B 63(13): 132104.

26. Liu CM, Chen XR, Xu C, Cai LC, Jing FQ (2012) Melting curves and entropy of fussion of body-centered cubic tungsten under pressure. Journal of Applied Physics 112: 013518.

27. Liu CM, Xu C, Cheng Y, Chen XR, Cai LC (2017) Molecular dynamics studies of body-centered cubic tungsten under pressure. Chinese Journal of Physics 55(6): 2468-2475.

28. Burakovsky L, Preston DL, Silbar RR (2000) Analysis of dislocation mechanism for melting of elements: Presure dependence. Journal of Applied Physics 88: 6294.

29. Guo Z, Yuan W, Sun Y, Cai Z, Qiao Z (2009) Thermodynamic assessment of the Si-Ta and Si-W systems. Journal of Phase Equilibria and Diffusion 30: 564.

30. Hoc NQ, Hien ND, Van CL, Dung NT, Ştefan Ţ (2021) Study on the melting temperature, the jumpings of volume, enthalpy and entropy at the melting point, and the Debye temperature for BCC defective and perfect interstitial alloy WSi under pressure. Journal of Composites Science 5: 153.

31. Cuong TD, Phan DA (2020) Modification of the statistical moment method for the high-pressure melting curve by the inclusion of thermal vacancies. Vacuum 179: 109444.

32. Zahroh FF, Sugihartono I, Safitri ED (2019) Young's modulus calculation of some metals using molecular dynamics method based on the Morse potential. Computational and Experimental Research in Materials and Renewable Energy (CERiMRE) 2(1): 19-34.

33. Raabe D, Roters F, Wang YW (2005) Simulation of earing during deep drawing of bcc steel by use of a texture component crystal plasticity finite element method. MSF 495-497: 1529-1534.

34. Zhang H, Punkkinen Marko PJ, Johansson B, Vitos L (2010) Theoretical elastic moduli of ferromagnetic bcc Fe alloys. Journal of Physics: Condensed Matter 22: 275402.

35. Vocadlo L, Price GD, Wood IG (1999) Crystal structure, compressibility and possible phase transitions in – FeSi studied by first-principles pseudopotential calculations. Acta Crystalographica Section B 55: 484-493.

36. Lau TT, Först CJ, Lin X, Gale JD, Yip S, et al. (2007) Many-body potential for point defect clusters in Fe-C alloys. Physical Review Letters 98(21): 215501.

37. Hallstedt B, Gröbner J, Hampl M, Schmid-Fetzer R (2016) Calometric measurements and assessment of the binary Cu-Si and ternary Al-Cu-Si diagrams. Calphad 53: 25-38.

38. Liyanage LSI, Kim SG, Houze J, Kim S, Tschopp MA, et al. (2014) Structural, elastic and thermal properties of cementite (Fe_3C) calculated using a modified embedded atom method. Physical Review B 89: 094102.

39. Tang N, Hung VV (1988) Investigation of the thermodynamic properties of anharmonic crystals by the momentum method, I. General results for face-centered cubic crystals. Physica Status Solidi (b) 149(2): 511-519.

40. Hùng VV (2009) Statistical moment method in studying thermodynamic and elastic properties of crystals. Hanoi National University of Education's Publishing House, Vietnam.

41. Tang N, Hung VV (1990) Investigation of the thermodynamic properties of anharmonic crystals by the momentum method, III. Thermodynamic properties of the crystals at various pressures. Physica Status Solidi (b) 162(2): 371-377.

42. Hung VV, Hoa NT (2006) Study of nonlinear deformation of metals. Communications in Physics 16(1): 18-25.

43. Hung VV, Hoa NT (2006) Nonlinear deformation of binary alloys investigated by statistical moment method. Communications in Physics 16(2): 121-128.

44. Magomedov MN (1987) On calculating the Debye temperature and the Gruneisen parameter. Zhurnal Fizicheskoi Khimii 61(4): 1003-1009.

45. Magomedov MN (2006) The calculation of the parameters of the Mie–Lennard-Jones potential. High Temperature 44(4): 513-529.

46. Magomedov MN (2006) The calculation of the parameters of the Mie–Lennard-Jones potential. Thermophysical Properties of Materials 44(4): 513-529.

47. Lide DR (2005) CRC Handbook of Chemistry and Physics. (86th edn.), Taylor & Francis, Boca Raton London, New York, Singapore.

48. Litasov KD, Gavryushkin PN, Dorogokupets PI, Sharygin IS, Shatskiy A, et al. (2013) Thermal equation of state to 33.5 GPa and 1673 K and thermodynamic properties of tungsten. Journal of Applied Physics 113: 133505.

49. Li W, Kou H, Zhang X, Ma J, Li Y, et al. (2019) Temperature-dependent elastic modulus model for metallic bulk materials. Mechanics of Materials 139: 103194.

50. Dwight EG (1961) American Institute of Physics Handbook. (2nd edn.), McGraw-Hill book Company, New York-Toronto-London.

51. Qi X, Cai N, Chen T, Wang S, Li B (2018) Experimental and theoretical studies on elasticity of tungsten to 13 GPa. Journal of Applied Physics 124(7): 075902.

52. Tikhonov LV, Knonenko GY (1986) Mechanical properties of metals and alloys. Kiev, Nauka Dumka, Ukraine.

53. Guo ZC, Luo F, Zhang XL, Yuan CY, Liu CA, et al. (2016) First-principles calculations of elastic, phonon and thermodynamic properties of W. Molecular Physics 114(23): 3430-3436.

54. Jiang D, Zhong S, Xiao W, Liu D, Wu M, et al. (2020) Structural, mechanical, electronic, and thermodynamic properties of pure tungsten metal under different pressures: A first-principles study. International Journal of Quantum Chemistry 120(13): e26231.

55. Xue L, Wang X, Xue F, Zhou X, Guo F, et al. (2021) Structural, mechanical, electronic properties and Debye temperature of tungsten-technetium alloy: A first-principles study. Fusion Engineering and Design 168: 112433.

56. Soderlind P, Eriksson O, Wills JM, Boring AM (1993) Theory of elastic constants of cubic transition metals and alloys. Physical Review B 48(9): 5844.

57. Einarsdotter K, Sadigh B, Grimvall G, Ozolins V (1997) Phonon instabilities in fcc and bcc tungsten. Physical Review Letters 79(11): 2073.

58. Viet LH, Hoc NQ (2021) Equilibrium vacancy concentration and thermodynamic quantities of FCC defective alloys AuCuSi and PtCuSi under pressure. HNUE Journal of Science, Natural Sciences 66(3): 38-51.